Glucose concentration monitoring using a small Fabry-Pérot etalon

Joerg Martini
Peter Kiesel
Jeffrey Roe
Richard H. Bruce
Palo Alto Research Center
3333 Coyote Hill Road
Palo Alto, California 94304
E-mail: joerg.martini@parc.com

Abstract. Accurate measurements of aqueous glucose concentrations have been made in a double-chamber Fabry-Pérot etalon that can be miniaturized for subcutaneous implantation to determine the concentration of glucose in interstitial fluid. In general, optical approaches to glucose detection measure light intensity, which in tissue varies due to inherent scattering and absorption. In our measurements, we compare the spectral positions of transmission maximums in two adjunct sections of an etalon in order to determine the refractive index difference between these sections and therefore we can tolerate large changes in intensity. With this approach, we were able to determine aqueous glucose concentrations between 0 mg/dl and 700 mg/dl within the precision of our reference measurement (±2.5 mg/dl or 2% of the measurement value). The use of reference cavities eliminates interference due to temperature variations, and we show the temperature independence over a temperature range of 32°C to 42°C. Furthermore, external filters eliminate interference from large molecule contaminants.
[DOI: 10.1117/1.3153848]

Keywords: refractive index; etalon; glucose detection; diabetes; continuous glucose monitoring (CGM); analyte assay; medical implant; vertical-cavity surface-emitting laser (VCSEL).

Paper 08390RR received Oct. 31, 2008; revised manuscript received Mar. 27, 2009; accepted for publication Apr. 14, 2009; published online Jun. 17, 2009.

1 Introduction

An analyte sensor that is accurate, reliable, and capable of continuous monitoring has a variety of medical applications. We demonstrate this capability with a double-chamber Fabry-Pérot etalon by monitoring the refractive index changes in various aqueous glucose mixtures. Glucose is important because of its link to diabetes. Studies show beneficial medical outcomes for diabetics utilizing present continuous glucose monitoring (CGM) systems.[1–4] Briefly, HbA_{1C} levels, hyperglycemic exposure, and hypoglycemic episodes are reduced. Tight glycemic control is correlated with reduced long-term health risks[5,6] such as kidney failure, cardiovascular diseases, loss of limbs and eyesight, as well as the immediate danger of hypoglycemic coma.[7] Glucose levels are affected by many factors in addition to food intake such as the metabolic state of the body, which is influenced by exercise, lag times in the digestive system, and the distribution of insulin in the body. Consequently, glucose levels vary widely and are difficult to predict. With CGM, measurements are made more frequently than with the standard procedure of infrequent blood withdrawals by finger stick tests. Consequently, important trend information is available to guide insulin dosage and carbohydrate intake.

The diagnostic gold standard is a measurement of glucose in a blood sample. This poses significant problems of accessibility for a CGM in a nonhospital setting due to risk of infection. Therefore, all FDA-approved minimally invasive CGM approaches measure glucose concentration in the interstitial fluid (ISF).[8] ISF components diffuse through the walls of blood vessels to and from the blood stream. In humans, this diffusion results in a several-minute latency between the ISF and blood glucose concentrations[9] that does not adversely affect the therapeutic value of CGM systems for diabetics.[1–4]

For over three decades, various noninvasive and minimally invasive techniques of CGM have been explored. Currently, the only FDA-approved CGM devices are based on an enzymatic reaction. This approach has several drawbacks that have limited its approved use to 7 days as an adjunct device not to be used for insulin adjustment. Due to low relative signal levels, the approach is least accurate at low glucose levels, where the signal to noise degrades. Because at low glucose levels patients face imminent danger, better sensitivity is needed. In addition, electrochemical devices are subject to sensor deterioration over time due to chemical and electrode aging.[10] For example, one product of the electrochemical reaction, hydrogen peroxide, denatures the active component of the sensor, glucose oxidase, and eventually destroys the device.[11] This approach is also susceptible to interference from molecules[12] such as acetaminophen, salicylates, uric acid (which can be more concentrated in people with diabetes), glutathione, ascorbic acid, and other reducing substances. Also, test results may be incorrect if the patient is severely

Address all correspondence to Joerg Martini, Hardware Systems Lab, Palo Alto Research Center, 3333 Coyote Hill Road, Palo Alto, CA 94304; Tel: 650 8124880; Fax: 650 8124251; E-mail: joerg.martini@parc.com

1083-3668/2009/14(3)/034029/8/$25.00 © 2009 SPIE

dehydrated, in shock, or in a hyperglycemic-hyperosmolar state, which can be life-threatening if not treated.

Because optical approaches circumvent these drawbacks, they offer a very attractive alternative method, especially in the 400-nm to 1600-nm wavelength region, where light sources and detectors are available, inexpensive, and small. However, despite decades of significant effort, no commercially successful optical detection system has been developed to measure glucose in bodily fluids continuously. Apparently, the optical characteristics of glucose[13–16] pose a significant problem for the development of a deployable, sensitive, and specific CGM system.

Zirk and Poetzschke[17,18] corrected this problem by demonstrating that refractive index (RI) measurements combined with filtering and conductivity measurements of blood plasma enable accurate glucose concentration measurements. The sensitivity is high because the glucose concentration variations have the largest influence on variations of the blood plasma's refractive index at our measure wavelength (850 nm). The problem of specificity was partially addressed using 30-kDa molecular weight cutoff (MWCO) filtering to remove large proteins, because their variation significantly alters the RI of the plasma. Zirk and Poetzschke address specificity to small molecules with two assumptions: they are primarily governed by the hydration level, and they are proportional to the ion concentration. They use conductivity measurements to determine the ion concentration, and from these measurements, they derive a correction factor that eliminates the effects of hydration. They were not able to eliminate the effects of temperature on the measurement, nor did they suggest a path to miniaturization needed for implantation.

In this paper, we present an RI measurement approach that addresses both the temperature and miniaturization limitations. We employ a design that contains reference chambers to eliminate effects of temperature and MWCO filtering to eliminate large-molecule interference.

2 Background

While the ISF's RI is dominated by its main constituent, water, it is affected by several of the ISF components such as proteins, small molecules, and glucose[13] as well as temperature. While changes in the glucose concentration have the strongest effect on the RI, changes in other ISF components have sufficiently significant effects on the RI[13] that they must be addressed. The RI change (at 589.3 nm) of glucose concentration accounts for $\Delta n = 1.41 \cdot 10^{-6}$ per 1 mg/dl glucose change.[19] This measurement compares to the value of $\Delta n = 1.43 \cdot 10^{-6}$ per 1 mg/dl that we measured at 785 nm with a commercial differential refractometer (Optilab rEX, Wyatt Technology). We have assumed a value of $\Delta n = 1.4 \cdot 10^{-6}$ per 1 mg/dl in the following estimations, lacking literature values for 850 nm. As the glucose concentration of diabetics should be detectable between 20 mg/dl and 600 mg/dl, a maximum RI change of $\Delta n = 8.4 \cdot 10^{-4}$ must be detectable. To achieve our target accuracy for clinical measurements of approximately ±3 mg/dl glucose, the RI needs to be measured to an accuracy of $\Delta n = \pm 4.2 \cdot 10^{-6}$. Note that the RI is strongly temperature dependent even within normal physiological temperature fluctuations. The variation in RI of water, $\Delta n = 1.4 \cdot 10^{-4}/°C$ in the physiological temperature range,[19] accounts for most of this temperature dependency. With the assumption that dn/dT is linear in the physiological temperature range and independent of the concentration of other ISF constituents, the temperature effect of 1 °C on the RI is equivalent to a glucose change of approximately 100 mg/dl. Therefore, temperature compensation is required.

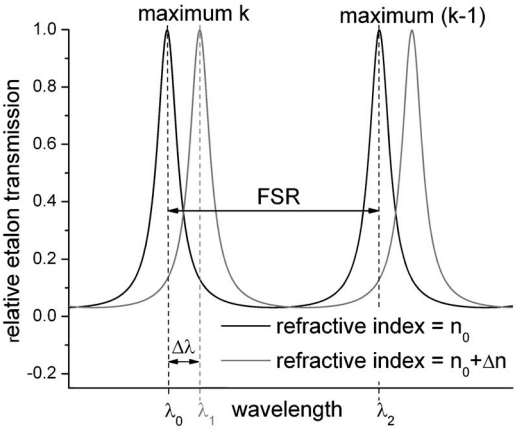

Fig. 1 Spectral position of FP modes for two different refractive indices. RI differences can be expressed by the normalized transmission shift $\Delta n = [n_0 \cdot (\lambda_1 - \lambda_0)]/[(k-1) \cdot (\lambda_2 - \lambda_0)]$, where k is the transmission order. For a linear wavelength sweep in time λ_0, λ_2 and λ_1 correspond to times t_0, t_2, and t_1.

A Fabry-Pérot interferometer (etalon) produces transmission maxima due to constructive interference and can be used to precisely measure changes in the refractive index of the material in the etalon cavity. This refractive index change is proportional to the shift in the transmission maxima normalized by the free spectral range (FSR), the wavelength difference between two successive maxima, as shown in Fig. 1. This shift is measured between two chambers of the same etalon where, for example, one chamber could open to ISF and the other remain sealed. The FSR of the etalon is chosen so that it is larger than the maximum RI shift induced by the maximum glucose concentration that we intend to measure (700 mg/dl). With this design, differences in FP-transmission peaks between the two chambers unambiguously specify the RI changes.

In our case, an etalon with 400-μm cavity thickness, filled with water, has an FSR of 680 pm with normal incident light at 850 nm, and it produces a wavelength shift of ~1 pm per 1 mg/dl glucose concentration. Measurement of such a shift requires use of a narrow-band light source and subpicometer wavelength accuracy. This requirement can be relaxed by sweeping a narrow-band light source linearly in time and by detecting the time-dependent transmission of the etalon chambers. The maximum transmission times t_0, t_2 in chamber 1 and t_1 in chamber 2 and the order k of the transmission maximum (an integer) determine the RI difference Δn of the two etalon chambers (see Fig. 1 and Appendix):

$$\Delta n = \frac{n_0 \cdot (t_1 - t_0)}{(k-1) \cdot (t_2 - t_0)}.$$

The normalized transmission shift $(t_1 - t_0)/(t_2 - t_0)$ is our measurement value. It varies between 0 and 1.

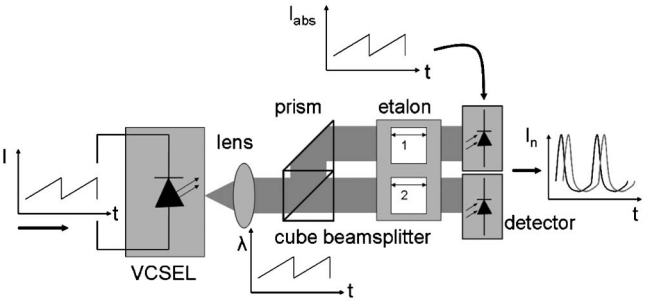

Fig. 2 Schematic experimental setup: The light from an 850-nm single-mode VCSEL is collimated and directed into a 50% beamsplitter. The incident beam is directed into one of the etalon's chambers (2), while the perpendicular beam is redirected by a prism into the other etalon chamber (1). The beams are parallel. The transmission of the etalon is detected by a two-segment PIN photodiode.

It is important to note that spectral linearity in time is sufficient to measure the RI difference without the knowledge of the light source's central wavelength or its exact time dependence (see Appendix).

Ambient temperature variations change the absolute spectral position of two neighboring transmission peaks. Their absolute position may vary by more than one FSR for possible physiological temperature changes due to the temperature dependency of the RI inside the cavity. In order to measure the FSR of the etalon's reference chamber under all circumstances, the light source's wavelength tuning range has to be sufficiently large, approximately 2.2 times the FSR. This enables the determination of the center position of at least two transmission peaks per chamber.

While the absolute spectral position of an etalon's transmission maxima has a strong temperature dependency due to the water content of the solution, the differential readout of the two chambers is dependent only on the temperature dependency of the RI difference Δn between the chambers. Assuming the same temperature dependency of aqueous glucose solutions as it is documented for aqueous maltose solutions[19] between 20°C and 25°C, the RI of a 100 mg/dl solution would change by $\Delta n = 1.3 \cdot 10^{-7}/°C$. This effect would result in a measurement error of $<0.1\%$ or <0.1 mg/dl and is therefore not relevant for physiological glucose concentration measurements.

3 Materials and Methods

We have constructed a prototype system (Fig. 2) that includes a two-chamber interferometer with a nominal mirror reflectivity of 70% and a mirror spacing of 400 μm. Both of the chambers can be filled separately with test liquids that are pumped from reservoirs. The chambers have lateral dimensions of 3 mm by 8 mm, and they are separated by 5 mm. We measured aqueous glucose solutions in the measurement chamber referenced to water in the reference chamber. We swept the wavelength of a commercial single-mode vertical-cavity surface-emitting laser (VCSEL, 850 nm) linearly across a range of 1470 pm with a modified sawtooth current pattern at 1 kHz. The probing laser light was collimated (2 mm diameter) and divided by a beamsplitter. The two parallel laser beams of approximately equal intensity were directed into the interferometer, as shown in Fig. 2. The full width at half maximum (FWHM) of the transmission peak in our setup is approximately 70 pm. This is consistent with the etalon finesse (<10), indicating that the spectral bandwidth of this commercially available VCSEL does not contribute significantly to the peak width and hence affect the resolution of the detector. A two-segment Si PIN photodiode detector (S5870, Hamamatsu Photonics, Hamamatsu, Japan) with a cutoff frequency of 10 MHz, measured the light transmission through the two interferometer chambers. Its signal was amplified by a transimpedance amplifier (10^4 V/A, −3-dB cutoff frequency >200 kHz). Data were collected at a 1-MHz rate over 300-ms intervals, resulting in 300 measurements of the normalized transmission shift between the chambers. We used the average of these measurements for all results that follow. The typical standard deviation of the 300 measurements remained under $2 \cdot 10^{-4}$. We also recorded the VCSEL intensity and used it to normalize the transmission intensities. Wavelength sweeping and transmission detection were performed with the same multifunction data acquisition board (PCI 6120, National Instruments, Austin, Texas); therefore, measurement synchronization between laser wavelength and the transmission intensity was relatively simple. This synchronization enabled correct assignment of transmission peaks.

Measurement control was performed by a LabView program, utilizing its peak detection function to determine the transmission peaks of the etalon chambers. Prior to our RI measurements, we adjusted the laser drive current function to ensure VCSEL wavelength linearity in time. Precise wavelength measurements are required in order to measure and adjust the linearity. We used a calibration etalon ($R_{1,2}=50\%$, $d=12$ mm) with a small FSR of 30 pm. We used the same detector, amplifier, and data acquisition board and found that our time resolution was sufficient to detect approximately 49 transmission maxima (1470-pm tuning range/30-pm FSR) in the calibration etalon across the wavelength tuning range of the VCSEL. The drive current function was adjusted until the positions of transmission maxima and minima were equidistant in time. This adjustment procedure was automated by a LabView program. The linearization of the wavelength sweep using adjusted current is shown Fig. 3(a). There, the temporal separation of successive transmission maxima and minima is displayed as a function of the laser sweep time. A constant temporal separation results in the laser wavelength sweep being linear in time. In Fig. 3(b), the wavelength shift, calculated from the separation of the transmission maxima and minima in Fig. 3(a), is plotted as a function of the laser sweep time. Figure 3(b) shows that the deviation from a linearity could be reduced from up to 24 pm for a linear drive current to <2.5 pm for the nonlinear VCSEL current. Note that our approach requires only linear temporal change in VCSEL wavelength. Accurate knowledge of the absolute VCSEL's wavelength is not needed. However, the linearization of the VCSEL wavelength sweep is necessary because a deviation of 1 pm results approximately in 1 mg/dl of apparent glucose concentration change

The VCSEL mount (LDM21, Thorlabs, Inc., Newton, New Jersey) used for thermal stabilization was also used to record the VCSEL temperature. While the VCSEL's wavelength changes significantly with temperature by 60 pm/°C, the re-

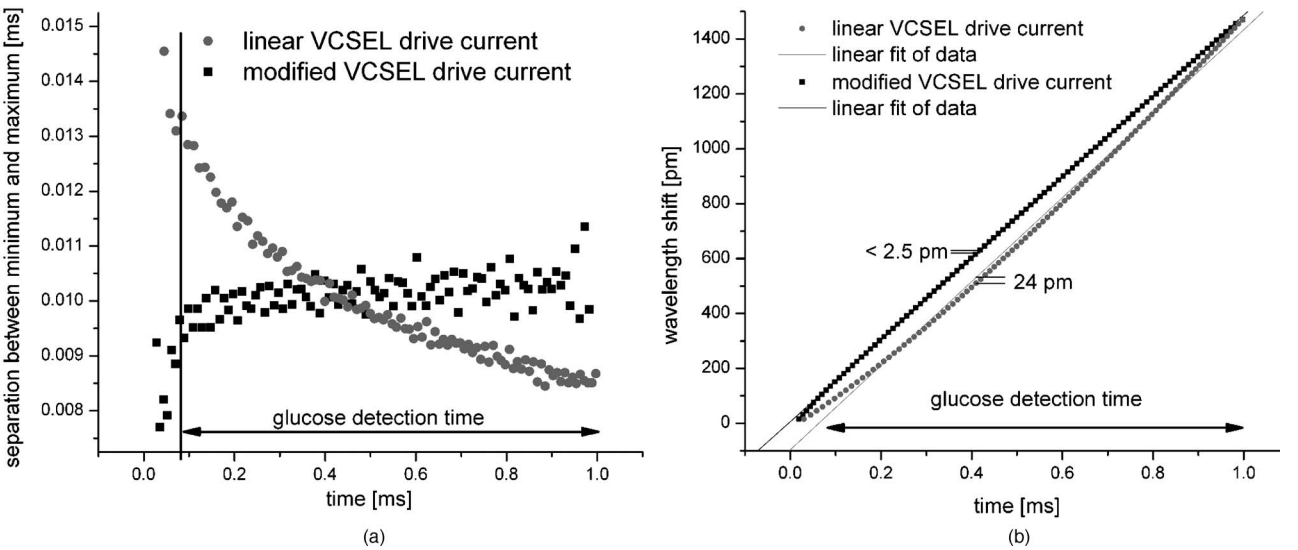

Fig. 3 VCSEL wavelength linearity in time. (a) The temporal separation between successive transmission minima and maxima is plotted against the sweep time. A constant temporal separation results in the laser wavelength sweep being linear in time. With a linear VCSEL drive current, the standard deviation of maximum–minimum transmission separation is $1.13 \cdot 10^{-3}$, while it is reduced to $5.31 \cdot 10^{-4}$ with the modified VCSEL drive current needed to produce a linear wavelength sweep. (b) The change in laser wavelength, calculated from the temporal separation of the transmission maxima and minima in (a), is plotted as a function of the laser sweep time. With a linear VCSEL drive current, the wavelength deviates from linearity up to 24 pm in the actual measurement range (0.08 ms to 1 ms). Using a nonlinear drive current, the deviation from linearity is less than 2.5 pm in the measurement range.

quired drive current function to guarantee wavelength linearity as discussed earlier showed surprisingly small variation. Figure 4 shows the temperature dependence of the VCSEL driving current function across the temperature range from 31 °C to 42 °C. We found that the same linearization function derived for 37 °C could be used over the entire temperature range without significant loss of accuracy by not taking data at low current values.

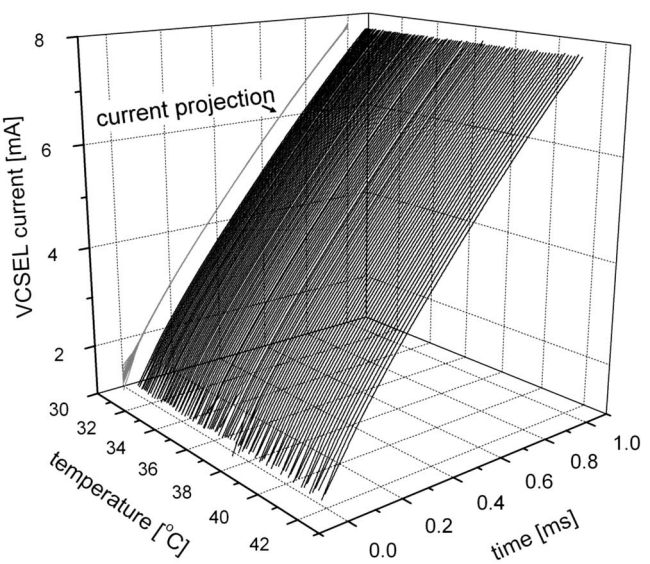

Fig. 4 A temperature dependence of the VCSEL driving current function that produces a linear wavelength change, the projection of all time-current curves reveals a surprisingly small variation in the function across the temperature range, deviations between the curves occur only at the onset of the driving pattern between 1 mA and 2 mA (0 ms to 0.08 ms), and data is not taken during this part of the current ramp.

Calibration of the system was made by comparing measurements of aqueous glucose samples using the etalon prototype with measurements made with a commercial glucose analyzer (YSI Model 2700G Glucose Analyzer, Yellow Springs Instrument Company, Yellow Springs, Ohio). Samples were prepared by volumetric dilution of a 1000 mg/dl stock solution made by dissolving α-D-Glucose (Calbiochem, La Jolla, California) into filtered deionized water (Milli-Q® Millipore, Billerica, Massachusetts). The RI-based concentration measurements were performed in an incubator at 37 °C. Twenty-five measurements were made over 2 min after both etalon chambers had reached temperature equilibrium and the measurement values were stable. The calibration and glucose concentration values were the average value of these measurements. The standard deviation remained smaller than $1.4 \cdot 10^{-4}$.

The calibration curve is shown in Fig. 5. The measured RI values depend linearly on the glucose concentration with a R^2 value of 0.9996; however, an offset of 0.256 was observed. Such an offset can be due to a divergence in the two probing beams or lack of parallelism in the etalon mirrors. A divergence of 1.15 deg between the beams could result in the observed shift as could a difference of approximately 80 nm between the average cavity spacing. In our case, beam divergence and etalon tilt contributed approximately equally to the observed offset. As long as the offset is stable over time, it will not reduce the sensitivity of the measurement. By subtracting this offset from the transmission shifts, the calibration curve can be used to measure glucose concentration values between 0 and 700 mg/dl.

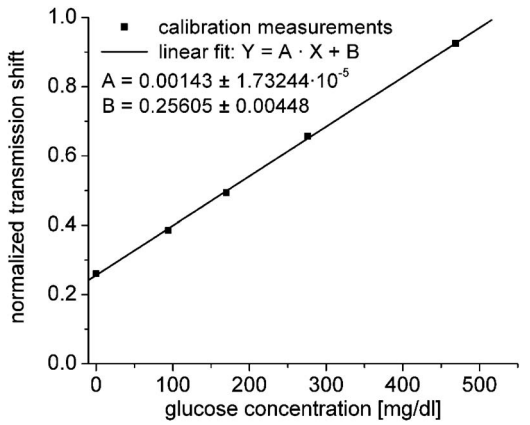

Fig. 5 Refractive index calibration curve. The change in refractive index is proportional to the transmission peak shift normalized by the free spectral range and varies linearly with the glucose concentration. The 25 measurements for each glucose concentration were carried out in 2 min, and their standard deviation remained smaller than $1.2 \cdot 10^{-4}$, while the accuracy of the reference measurement was ±2.5 mg/dl, or 2% of the measurement. In addition to the results of the linear fit for the calibration data, the standard error of the fit is displayed.

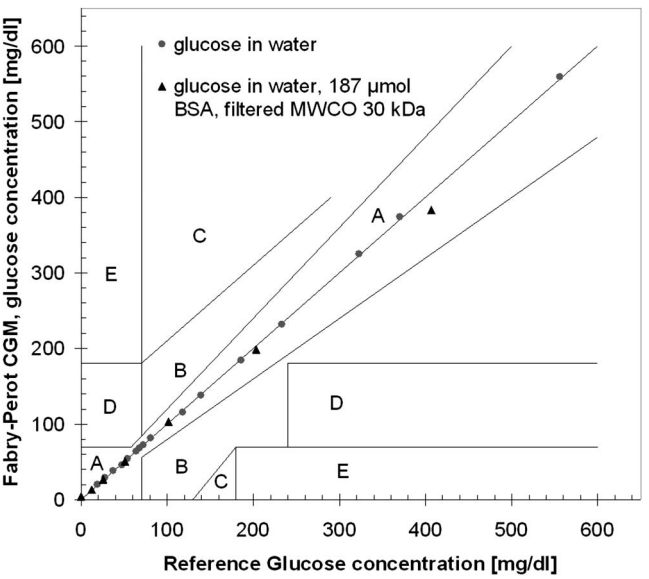

Fig. 6 Aqueous glucose concentration measurements: Gray circles represent measurements of different glucose solutions, and black triangles represent measurements of glucose solutions in the presence of 187 μmol/l BSA that were filtered by a 30-kDa MWCO membrane. The 25 measurements for each glucose concentration were carried out in 2 min, and their standard deviation remained smaller than ±0.1 mg/dl, while the accuracy of the reference measurement was ±2.5 mg/dl, or 2% of the measurement. In order to demonstrate the clinical relevance of measurement errors, a Clarke error grid is superimposed on the data, which is a common representation for medical glucose meters. Zone A: Clinically accurate; would lead to correct treatment decisions. Zone B: Would lead to benign decisions or no treatment. Zone C: Would lead to overcorrection of normal glucose levels. Zone D: Would lead to failure to detect and treat high or low glucose levels. Zone E: Would lead to erroneous treatment decisions.

Bovine serum albumin (BSA, Fraction V, OmniPur, EMD Chemicals, Inc., Gibbstown, New Jersey) was dissolved in filtered deionized water. Protein concentrations of the stock solution were prepared gravimetrically and validated by absorption spectroscopy at 280 nm. Glucose-BSA aqueous solutions were prepared by adding glucose solutions of various concentrations to the BSA stock solution in a 1-to-1 volume ratio.

These samples were subsequently filtered with 30-kDa MWCO centrifugal filters (Amicon Ultra 15, Millipore, Billerica, Massachusetts). The filters were prepared by rinsing them with deionized water twice at 20°C and 3000 g for 5 min. BSA filtering was done at 20°C and 3000 g for 15 min. The filtrate was subsequently used to determine its BSA content by absorption spectroscopy and for refractive index measurements in our double-chamber etalon. The BSA concentrations of the filtrate remained below the detection limit of the absorption spectrometer (DU 530, Beckman Instruments, Inc., Fullerton, California).

4 Results

All glucose measurements made with our prototype device are within the precision of reference measurements made with the YSI instrument (Table 1). Furthermore, all measurements are located within the optimal region of the Clarke error grid, as shown in Fig. 6. This plot represents a graphical method to illustrate the clinical implications of measurement errors.[20] The optimal region represents clinically accurate measurements that would lead to correct treatment decisions.

To validate Zirk and Poetzschke's finding[18] that a MWCO filter can effectively eliminate large molecule contamination, we made measurements of samples that contained bovine serum albumin (BSA) that were filtered with a 30-kDa MWCO filter prior to the measurement. We used a concentration of 187-μM BSA concentration, which would have the same influence on the RI as 1640 mg/dl glucose. As can be seen in

Table 1 Measured values of glucose for different concentrations of glucose dissolved in water. The standard deviation of 25 etalon measurements performed in 2 min resulted in a typical precision of ±0.1 mg/dl. The top row lists measurements made with a commercial glucose meter along with its published precision, and the bottom row lists measurements made with our etalon detector prototype. All of the etalon measurements fall within the error bars of the reference measurements.

Glucose reference (mg/dl)	18.7 ±2.5	64.4 ±2.5	68.1 ±2.5	72.4 ±2.5	81.1 ±2.5	139 ±2.8	233 ±4.7	323 ±6.5	556 ±11.1
Etalon glucose measurement (mg/dl)	19.8	63.9	68.2	72.2	81.3	138.3	231.9	324.9	559.3

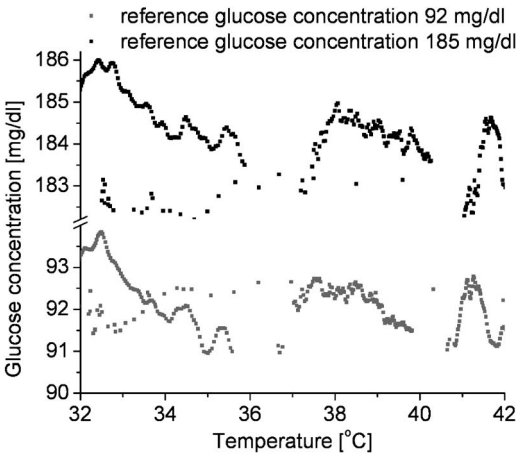

Fig. 7 Temperature dependency of two glucose readings. The observed deviations from the nominal value are small and can be even further improved since the observed deviations are clearly systematic. Mean values and standard deviation across the temperature region are 91.9±1.04 mg/dl and 184.34±1.09 mg/dl.

Fig. 6, the BSA concentration did not affect the RI measurements, and filtering is an effective method for eliminating large molecule concentration.

We tested the inherent temperature compensation by varying the ambient temperature of the prototype sensor's environment. The temperature was measured by a thermistor attached to the sensor unit. The VCSEL was not additionally temperature stabilized, so VCSEL and chamber were exposed to the same temperature variations. We measured two glucose concentrations in water (YSI reference: 92 mg/dl and 185 mg/dl; etalon measurement average: 92 mg/dl and 184 mg/dl) across the temperature range of 32°C to 42°C. As shown in Fig. 7, the standard deviation of the measurements across the range remained small (~1 mg/dl). Note that without the compensation from the reference chamber, an absolute measured RI change would have yielded an apparent glucose concentration change by 1000 mg/dl across this temperature range. Therefore, we have no indication that either the slope or the offset of the etalon's calibration (Fig. 5) change significantly as a function of temperature. We did not see significant changes in slope or offset over the course of our measurements (~8 hours); therefore, they are inherent to the etalon and the beam alignment.

Furthermore, when comparing both measurements, it seems that there are systematic errors in the measurement that are correlated with temperature. As the measurements were taken several hours apart from one another and little noise seems to be present, thermal expansion of the materials in the measurement setup—in particular, the etalon—seems an unlikely explanation for the fluctuations in the measurements. We expect that the small apparent temperature dependency could be reduced if necessary by using different VCSEL drive current patterns for each temperature; however, the glucose sensitivity is sufficient for an implantable glucose detector.

5 Discussion

In this paper, we show that a double-chamber etalon approach can make very precise glucose measurements such that all of our measurement results are within the error margin of reference measurements obtained with a commercial instrument (2.5 mg/dl or 2%, whichever is larger). All of our measurements fell into the A region of the Clarke error grid. Therefore, the inherent accuracy and precision of our measurement is more than sufficient for CGM.

We confirmed that large molecule interference can be eliminated by MWCO filtering. We further show that the double-chamber device has adequate inherent temperature compensation, allowing a standard deviation of ±1 mg/dl across a temperature variation of 10°C, a generous physiological temperature range.

While these results are promising, several considerations need to be addressed for a functioning CGM. These include specificity to small molecules, reduced implant size, sensor measurement latency, and power consumption. We are currently testing two approaches for implementing small molecule specificity. One is measuring the ISF conductivity which according to Zirk and Poetzschke,[18] limits inaccuracies of glucose concentration measurements to less than 10%, fulfilling the ISO 15197 guidelines for self-testing blood glucose monitoring systems. Here we have to thoroughly test the assumption that the small molecule concentration is mainly affected by hydration level and can be determined by measuring the ion concentration through conductivity measurements. A potentially more accurate approach is using a reversible affinity reaction with a glucose-specific receptor such as Concanavalin A (ConA) and a ligand such as dextran.[21–24] In such a reaction, ConA is released from dextran through binding with glucose so that the ConA concentration is proportional to the glucose concentration. Since ConA is much larger than glucose, it produces a substantially larger change in the refractive index. As ConA is a carbohydrate-specific binder, other small molecules such as lactic acid or NaCl should not interact with ConA, so the mechanism is inherently glucose specific.

The double-chamber device can be miniaturized using microfabrication techniques. A device design that incorporates MWCO filtering as well as conductivity and RI measurements is shown in Fig. 8. The device will consist of a two-chamber etalon that operates like the prototype described for this paper. Here, the reference chamber is filled with water or a glucose mixture and sealed so that its RI does not change. The measurement chamber is exposed to ISF through MWCO membranes that prevent large interfering ISF components from entering the chamber. The membranes also protect the optical surfaces of the interferometer's mirrors from interfering deposits of cells and proteins.

To enable a low latency response, fast diffusion times are needed through the MWCO filters. This is accomplished by using filters with a high diffusivity and a high surface-to-volume ratio (40 cm^{-1}). The surface-to-volume ratio is achieved with a small device having chamber size of 0.5 mm × 1 mm × 0.4 mm. The membranes are located on three open sides of the chambers, while top and bottom contain the reflective coatings that form the etalon. Biocompatible membranes[25,26] that meet our MWCO filter requirements are available with a diffusivity of $1.1 \cdot 10^{-7}$ to $3.2 \cdot 10^{-8}$ cm^2/s for a small molecule such as glucose. Diffusion-time constants for glucose diffusing through

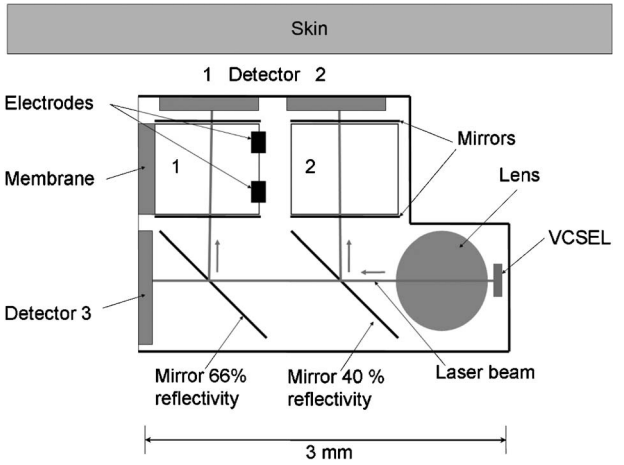

Fig. 8 Schematic design of an implantable CGM. Light from the VCSEL is collimated by a ball lens and reflected by partially reflecting mirrors through the etalon. The detectors detect transmission peaks of light passing through the two etalon chambers. An MWCO membrane prevents large molecules from entering the measurement chamber (1) that could optionally contains electrodes for making a conductivity measurement. The reference chamber (2) is sealed. A third detector is used to monitor the laser intensity. The device can be miniaturized using microfabrication to be implantable size.

these membranes then range between 6.5 to 10 min for a membrane thickness of 25 μm. The two electrodes required for conductivity measurements are contained in the measurement chamber.

The size of the VCSEL dice that has been used in our setup is 250 μm $\times$ 250 μm $\times$ 150 μm. Furthermore, PIN-diode detector dice are available in the required size of the etalon's chambers. Therefore, size and spectral requirements of the laser can be readily met with commercially available devices. Consequently, an implanted device could include both the laser and detectors integrated into a small package, with dimensions 4.5 mm $\times$ 3 mm $\times$ 3 mm. We expect that such a substantial reduction in size and the gluing of all the optical components should additionally reduce thermally induced mechanical stress. Furthermore, we expect that external pressure on the device will result in a displacement of the whole implant and not an asymmetrical deformation of the chambers. The operational power requirements of the VCSEL (8 mW), detection electronics (15 mW), and electronics (25 mW running and 50 μW standby) are modest. We estimate that about 0.05 mW is needed for one measurement every 5 min, which is a reasonable duty cycle for glucose detection. This power can be provided through inductive power transfer through the skin.[27]

The detector has several characteristics that should help to make it biocompatible. Fundamentally, it is an inert device containing no consumables and producing no contaminating by-products. It is constructed from inorganic materials and can be easily encapsulated in hydrogel[28] or other biocompatible materials[29] to minimize inflammation. Vascularization reagents[30,31] can be used to promote capillary formation in its vicinity to eliminate encapsulation that leads to increased latency.

Appendix

An ideal etalon's transmission is determined by the cavity characteristics[32]:

$$T = \frac{(1-R_1-A_1)\cdot(1-R_2-A_2)\cdot\exp(-\alpha d)}{[1-\sqrt{R_1R_2}\cdot\exp(-\alpha d)]^2} \cdot \frac{1}{1+\frac{4\sqrt{R_1R_2}\cdot\exp(-\alpha d)}{[1-\sqrt{R_1R_2}\cdot\exp(-\alpha d)]^2}\cdot\sin^2\left(\frac{2\pi n d\cos\theta}{\lambda}\right)}, \tag{1}$$

where T is the relative etalon transmission $R_{1,2}$ are the mirror reflectivities; $A_{1,2}$ are the mirror absorptions; α is the absorption coefficient of the material, and n is the refractive index of material in the cavity for wavelength λ; and d is the thickness of the cavity, and θ is the angle of incident light.

From Eq. (1), it can be inferred that the spectral position of the etalon's transmission maxima, which are also known as Fabry-Pérot modes (FP-modes), have to fulfill:

$$k\cdot\lambda = 2\cdot d\cdot n\cdot\cos\theta, \tag{2}$$

where k is an integer.

From Eq. (2), it is obvious that the spectral position of an individual FP-mode provides a measurement for the RI inside a given etalon. This is the underlying principle of the approach we are presenting in this paper.

With Eq. (2), the spectral position of the FP-modes for different refractive indices n_0 and $n_0+\Delta n$ in Fig. 1 may be expressed as:

$$\lambda_1-\lambda_0 = \frac{2\cdot d\cdot\Delta n\cdot\cos\theta}{k} \Leftrightarrow \Delta n = \frac{k}{2\cdot d\cdot\cos\theta}\cdot(\lambda_1-\lambda_0). \tag{3}$$

In the same manner, the free spectral range of an etalon is defined as the spectral distance between two neighboring FP-modes (see Fig. 1, λ_0 and λ_2), which may be expressed as:

$$\lambda_2-\lambda_0 = \frac{2\cdot d\cdot n_0\cdot\cos\theta}{k-1} - \frac{2\cdot d\cdot n_0\cdot\cos\theta}{k} = \frac{2\cdot d\cdot n_0\cdot\cos\theta}{k(k-1)} \Leftrightarrow \frac{k}{2\cdot d\cdot\cos\theta} = \frac{n_0}{(k-1)\cdot(\lambda_2-\lambda_0)}. \tag{4}$$

Hence, by combining Eq. (3) and Eq. (4), the difference in RI in an etalon can be expressed as:

$$\Delta n = \frac{n_0\cdot(\lambda_1-\lambda_0)}{(k-1)\cdot(\lambda_2-\lambda_0)}. \tag{5}$$

It has to be appreciated that Eq. (5) is now independent of beam alignment and etalon properties.

Wavelength detection would have to be precise to the subpicometer scale for our application. This can be circumvented by sweeping a narrow-band light source linearly in time:

$$\lambda(t) = \lambda_C + h \cdot t. \quad (6)$$

By detecting the etalon's transmission in time and recording the maximum transmission times t_0, t_1, and t_2 (corresponding to λ_0, λ_1, and λ_2 in Fig. 1), Eq. (5) simplifies to:

$$\Delta n = \frac{n_0 \cdot (t_1 - t_0)}{(k-1) \cdot (t_2 - t_0)}. \quad (7)$$

It has to be pointed out that the requirement of spectral linearity in time is sufficient to measure the RI difference Δn without the knowledge of the light source's central wavelength [λ_C in Eq. (6)] or its slope in time [h in Eq. (6)]. The measurement value $(t_1\text{-}t_0)/(t_2\text{-}t_0)$ in Eq. (7) can then be regarded as a normalized transmission shift that varies between 0 and 1.

References

1. S. L. Ellis, R. G. Naik, K. Gemperline, and S. K. Garg, "Use of continuous glucose monitoring in patients with type 1 diabetes," *Curr. Diabetes Rev.* **4**(3), 207–217 (2008).
2. H. R. Murphy, G. Rayman, K. Lewis, S. Kelly, B. Johal, K. Duffield, D. Fowler, P. J. Campbell, and R. C. Temple, "Effectiveness of continuous glucose monitoring in pregnant women with diabetes: randomised clinical trial," *Br. Med. J.* **337**, a1680 (2008).
3. R. Zick, B. Petersen, M. Richter, and C. Haug, "Comparison of continuous blood glucose measurement with conventional documentation of hypoglycemia in patients with type 2 diabetes on multiple daily insulin injection therapy," *Diabetes Technol. Ther.* **9**(6), 483–492 (2007).
4. W. V. Tamborlane, R. W. Beck, B. W. Bode, B. Buckingham, H. P. Chase, R. Clemons, R. Fiallo-Scharer, L. A. Fox, L. K. Gilliam, I. B. Hirsch, E. S. Huang, C. Kollman, A. J. Kowalski, L. Laffel, J. M. Lawrence, J. Lee, N. Mauras, M. O'Grady, K. J. Ruedy, M. Tansey, E. Tsalikian, S. Weinzimer, D. M. Wilson, H. Wolpert, T. Wysocki, and D. Xing, "Continuous glucose monitoring and intensive treatment of type 1 diabetes," *N. Engl. J. Med.* **359**(14), 1464–1476 (2008).
5. The Diabetes Control and Complications Trial Research Group, "The effect of intensive treatment of diabetes on the development and progression of long-term complications in insulin-dependent diabetes mellitus," *N. Engl. J. Med.* **329**(14), 977–986 (1993).
6. UK Prospective Diabetes Study (UKPDS) Group, "Intensive blood-glucose control with sulphonylureas or insulin compared with conventional treatment and risk of complications in patients with type 2 diabetes (UKPDS 33)," *Lancet* **352**(9131), 837–853 (1998).
7. P. E. Cryer, S. N. Davis, and H. Shamoon, "Hypoglycemia in diabetes," *Diabetes Care* **26**(6), 1902–1912 (2003).
8. V. R. Kondepati and H. M. Heise, "Recent progress in analytical instrumentation for glycemic control in diabetic and critically ill patients," *Anal. Bioanal. Chem.* **388**(3), 545–563 (2007).
9. K. Rebrin, G. M. Steil, W. P. van Antwerp, and J. J. Mastrototaro, "Subcutaneous glucose predicts plasma glucose independent of insulin: implications for continuous monitoring," *Am. J. Physiol.* **277**(3 Pt 1), E561–E571 (1999).
10. T. I. Valdes and F. Moussy, "*In vitro* and *in vivo* degradation of glucose oxidase enzyme used for an implantable glucose biosensor," *Diabetes Technol. Ther.* **2**(3), 367–376 (2000).
11. E. Wilkins and P. Atanasov, "Glucose monitoring: state of the art and future possibilities," *Med. Eng. Phys.* **18**(4), 273–288 (1996).
12. G. Ramsay, "Commercial biosensors: Applications to clinical, bioprocess and environmental samples," in *Chemical Analysis*, J. D. Winefordner, Ed., John Wiley & Sons, New York (1998).
13. O. S. Khalil, "Spectroscopic and clinical aspects of noninvasive glucose measurements," *Clin. Chem.* **45**(2), 165–177 (1999).
14. A. Tura, A. Maran, and G. Pacini, "Non-invasive glucose monitoring: assessment of technologies and devices according to quantitative criteria," *Diabetes Res. Clin. Pract.* **77**(1), 16–40 (2007).
15. R. J. McNichols and G. L. Cote, "Optical glucose sensing in biological fluids: an overview," *J. Biomed. Opt.* **5**(1), 5–16 (2000).
16. G. L. Cote, "Noninvasive and minimally invasive optical monitoring technologies," *J. Nutr.* **131**(5), 1596S–1604S (2001).
17. K. Zirk and H. Poetzschke, "On the suitability of refractometry for the analysis of glucose in blood-derived fluids," *Med. Eng. Phys.* **26**(6), 473–481 (2004).
18. K. Zirk and H. Poetzschke, "A refractometry-based glucose analysis of body fluids," *Med. Eng. Phys.* **29**(4), 449–458 (2007).
19. R. C. Weast, Ed., *CRC Handbook of Chemistry and Physics*, CRC, Cleveland, OH (1971).
20. W. L. Clarke, D. Cox, L. A. Gonder-Frederick, W. Carter, and S. L. Pohl, "Evaluating clinical accuracy of systems for self-monitoring of blood glucose," *Diabetes Care* **10**(5), 622–628 (1987).
21. B. B. Agrawal and I. J. Goldstein, "Specific binding of concanavalin A to cross-linked dextran gels," *Biochem. J.* **96**(3), 23c–25c (1965).
22. B. B. Agrawal and I. J. Goldstein, "Protein-carbohydrate interaction. VI. Isolation of concanavalin A by specific adsorption on cross-linked dextran gels," *Biochim. Biophys. Acta* **147**(2), 262–271 (1967).
23. J. L. Wang and G. M. Edelman, "Binding and functional properties of concanavalin A and its derivatives. I. Monovalent, divalent, and tetravalent derivatives stable at physiological pH," *J. Biol. Chem.* **253**(9), 3000–3007 (1978).
24. R. Ballerstadt and J. S. Schultz, "A fluorescence affinity hollow fiber sensor for continuous transdermal glucose monitoring," *Anal. Chem.* **72**(17), 4185–4192 (2000).
25. C. Smith, R. Kirk, T. West, M. Bratzel, M. Cohen, F. Martin, A. Boiarski, and A. A. Rampersaud, "Diffusion characteristics of microfabricated silicon nanopore membranes as immunoisolation membranes for use in cellular therapeutics," *Diabetes Technol. Ther.* **7**(1), 151–162 (2005).
26. H. R. Kermis, G. Rao, and T. A. Barbari, "Transport properties of pHEMA membranes for optical glucose affinity sensors," *J. Membr. Sci.* **212**(1–2), 75–86 (2003).
27. M. Catrysse, B. Hermans, and R. Puers, "An inductive power system with integrated bi-directional data-transmission," *Sens. Actuators, A* **115**(2–3), 221–229 (2004).
28. B. Yu, C. Wang, Y. M. Ju, L. West, J. Harmon, Y. Moussy, and F. Moussy, "Use of hydrogel coating to improve the performance of implanted glucose sensors," *Biosens. Bioelectron.* **23**(8), 1278–1284 (2008).
29. Y. M. Ju, B. Yu, T. J. Koob, Y. Moussy, and F. Moussy, "A novel porous collagen scaffold around an implantable biosensor for improving biocompatibility. I. *In vitro*/*in vivo* stability of the scaffold and *in vitro* sensitivity of the glucose sensor with scaffold," *J. Biomed. Mater. Res. Part A* **87**(1), 136–146 (2008).
30. U. Klueh, D. I. Dorsky, and D. L. Kreutzer, "Enhancement of implantable glucose sensor function *in vivo* using gene transfer-induced neovascularization," *Biomaterials* **26**(10), 1155–1163 (2005).
31. W. K. Ward, M. J. Quinn, M. D. Wood, K. L. Tiekotter, S. Pidikiti, and J. A. Gallagher, "Vascularizing the tissue surrounding a model biosensor: how localized is the effect of a subcutaneous infusion of vascular endothelial growth factor (VEGF)?" *Biosens. Bioelectron.* **19**(3), 155–163 (2003).
32. W. Vogel, M. Berroth, and G. C. Righini, "Tunable liquid crystal Fabry-Pérot filters," *Proc. SPIE* **4944**, 293–302 (2003).